AFRL-RX-WP-TP-2012-0390

DETERMINATION OF γ'SITE OCCUPANCIES IN NICKEL SUPERALLOYS USING ATOM PROBE TOMOGRAPHY AND X-RAY DIFFRACTION (PREPRINT)

J. Tiley, O. Senkov, and G. Viswanathan
Metals Branch
Structural Materials Division

S. Nag and R. Banerjee
University of North Texas

J.Hwang
Institute of Advanced Composite Materials
Korea Institute of Science and Technology

AUGUST 2012
Interim

AIR FORCE RESEARCH LABORATORY
MATERIALS AND MANUFACTURING DIRECTORATE
WRIGHT-PATTERSON AIR FORCE BASE, OH 45433-7750
AIR FORCE MATERIEL COMMAND
UNITED STATES AIR FORCE

REPORT DOCUMENTATION PAGE

Form Approved
OMB No. 0704-0188

1. REPORT DATE *(DD-MM-YY)*	2. REPORT TYPE	3. DATES COVERED *(From - To)*
August 2012	Technical Paper	1 July 2012 – 1 August 2012

4. TITLE AND SUBTITLE

DETERMINATION OF γ'SITE OCCUPANCIES IN NICKEL SUPERALLOYS USING ATOM PROBE TOMOGRAPHY AND X-RAY DIFFRACTION (PREPRINT)

5a. CONTRACT NUMBER
FA8650-08-C-5226

5b. GRANT NUMBER

5c. PROGRAM ELEMENT NUMBER
62102F

6. AUTHOR(S)

J. Tiley, O. Senkov, and G. Viswanathan (AFRL/RXCM)
S. Nag and R. Banerjee (University of North Texas)
J.Hwang (Institute of Advanced Composite Materials, Korea Institute of Science and Technology)

5d. PROJECT NUMBER
4347

5e. TASK NUMBER

5f. WORK UNIT NUMBER
X06B

7. PERFORMING ORGANIZATION NAME(S) AND ADDRESS(ES)

University of North Texas
Corner of Ave C Chestnut
Denton, TX 76203

8. PERFORMING ORGANIZATION REPORT NUMBER
AFRL-RX-WP-TP-2012-0390

9. SPONSORING/MONITORING AGENCY NAME(S) AND ADDRESS(ES)

Air Force Research Laboratory
Materials and Manufacturing Directorate
Wright-Patterson Air Force Base, OH 45433-7750
Air Force Materiel Command
United States Air Force

10. SPONSORING/MONITORING AGENCY ACRONYM(S)
AFRL/RXCM

11. SPONSORING/MONITORING AGENCY REPORT NUMBER(S)
AFRL-RX-WP-TP-2012-0390

12. DISTRIBUTION/AVAILABILITY STATEMENT

Approved for public release; distribution unlimited. Preprint to be submitted to Metallurgical and Materials Transactions.

13. SUPPLEMENTARY NOTES

The U.S. Government is joint author of this work and has the right to use, modify, reproduce, release, perform, display, or disclose the work. PA Case Number and clearance date: 88ABW-2012-2970, 21 May 2012. This document contains color.

14. ABSTRACT

Rene88 samples were investigated using atom probe tomography and x-ray diffraction using a monochromated synchrotron beam with different energy values to determine the preferred site occupancy of various alloying elements within the ordered γ' precipitates. Samples were solutionized and cooled at 24 degree C/min with subsequent aging at 760 degrees C. The synchrotron-based x-ray diffraction results indicate that niobium prefers to reside on the aluminum sublattice site of the γ' phase. Additionally, the experimental results also indicate that chromium prefers the nickel sublattice sites while cobalt is likely to occupy both the aluminum and nickel sublattice sites. The x-ray results on the chromium occupancy disagree with atom probe results from the same alloy that indicate that chromium prefers the aluminum sublattice sites. Modeling studies indicate cobalt has no strong site preference.

15. SUBJECT TERMS

site occupancy, chemical segregation, atom probe tomography

16. SECURITY CLASSIFICATION OF:			17. LIMITATION OF ABSTRACT:	NUMBER OF PAGES	19a. NAME OF RESPONSIBLE PERSON (Monitor)
a. REPORT	b. ABSTRACT	c. THIS PAGE			Jaimie Tiley
Unclassified	Unclassified	Unclassified	SAR	18	19b. TELEPHONE NUMBER *(Include Area Code)* N/A

Determination of γ' Site Occupancies in Nickel Superalloys using Atom Probe Tomography and X-ray Diffraction

J. Tiley[1], O. Senkov[1], G. Viswanathan[1], S. Nag[2], J. Hwang[3], R. Banerjee[2]

[1] Air Force Research Laboratory, Wright Patterson AFB OH 45433
[2] Center for Advanced Research and Technology and Department of Materials Science, University of North Texas, Denton TX 76203
[3]Institute of Advanced Composite Materials, Korea Institute of Science and Technology, Jeonbuk, 565-902, Korea

Abstract

Rene88 samples were investigated using atom probe tomography and x-ray diffraction using a monochromated synchrotron beam with different energy values to determine the preferred site occupancy of various alloying elements within the ordered γ' precipitates. Samples were solutionized and cooled at 24 degree C/min with subsequent aging at 760 degrees C. The synchrotron-based x-ray diffraction results indicate that niobium prefers to reside on the aluminum sublattice site of the γ' phase. Additionally, the experimental results also indicate that chromium prefers the nickel sublattice sites while cobalt is likely to occupy both the aluminum and nickel sublattice sites. The x-ray results on the chromium occupancy disagree with atom probe results from the same alloy that indicate that chromium prefers the aluminum sublattice sites. Modeling studies indicate cobalt has no strong site preference.

Introduction

Nickel base super alloys are used in many high temperature aerospace applications where their excellent strength and creep properties are required [1,2,3,4,5]. For many of these alloy systems, the formation of an $L1_2$ ordered fcc phase (γ') within the fcc parent phase (γ) is critical for mechanical properties. The formation of γ' has been extensively studied [5,6,7,8] and linked to numerous properties, including creep [9,10] strength and fatigue [11,12]. Researchers have identified the corresponding changes in deformation mechanisms as a function of temperature and microstructure [8,9]. This is critical, since the operational temperature for the components using these alloys continues to increase. Given the importance of microstructure on mechanical behavior, it is not surprising that numerous studies have investigated the nucleation, growth and coarsening of γ' precipitates [13,14,15]. Because the models for these mechanisms rely on the volume fraction of γ'and the transition from growth to coarsening mechanisms, x-ray diffraction

techniques are often employed to determine key microstructure parameters [16,17]. Unfortunately, for complex commercial nickel base superalloys, exact site occupancy data within γ' is extremely difficult to obtain and verify experimentally. Chemical segregation between γ and γ' has been successfully studied and reported for a number of nickel base superalloys using computational approaches involving energy potentials, and alloying element segregation to either Al or Ni sites with γ' has been modeled for ternary alloy systems[18,19,20,21,22]. However, for alloy systems with more than a few different alloying elements, it becomes computationally difficult to determine energies for accurate site occupancy estimations, and experimentally difficult to apply transmission electron diffraction and Rietveld refinement using either neutron and/or x-ray diffraction techniques. Given the number of potential interactions between the elements and lattice positions, the problem is over determined and potentially mathematically non-unique.

Atom probe tomography (APT) has been successfully used to address the problem of identifying chemical segregation in nickel-base superalloys with multiple alloying elements [23,24,25,26]. Furthermore, APT techniques have been directly applied to the investigation of γ' formation and growth/coarsening [27,28]. Although this work has provided considerable insights into the morphological and compositional evolution of γ'precipitates, the techniques are limited by volume constraints on the amount of material evaluated, and the by spatial resolution, making it difficult to determine specific site occupancies. A complimentary technique involves dissolving away the matrix γ' and using x-ray diffraction techniques to evaluate the residual powders (after they have been dried) [13]. Although this allows the direct evaluation of unconstrained γ', it does not provide the site occupancies for alloying elements.

Rene88 is a widely-used commercial nickel base superalloy with a 42.5 volume% γ' content, used primarily in propulsion systems [13]. The material has a low γ/γ' misfit and γ' solvus of approximately 1124 degrees C, making it an ideal alloy for comparing the effects of heat treatment on phase evolution with other third generation nickel base superalloys [29,30]. Researchers have shown that the alloy forms different distributions of γ' dependent on the cooling rates used in heat treatments [7,13]. Further analysis of γ' coarsening provided insight into the behavior of the phases when aged at 760 degrees C for up to 200 hours [7,14,31]. The results indicated the importance of diffusion across the interface and the impact of solute pile-

ups. Although researchers were able to use energy filtered transmission electron microscopy techniques and x-ray diffraction studies to image and determine the volume fraction of γ' within aged Rene88, they used chemical composition data provided by atom probe tomography [31], which relied on a narrow statistical data set of γ' precipitates. Researchers were unable to build complete models of the γ' phases using their data because the exact site occupancies within γ' were unknown since it is very difficult to determine from the atom probe data .

One promising approach to determine the site occupancies (and subsequently model the bulk microstructure properties including volume fraction of γ') involves the Rietveld refinement of diffraction data. Modeling of peak intensities for different phase compositions provides a method of determining the most likely site occupancies. However, within γ', the elements change occupancy between Ni and Al sites depending on their neighbors [18] especially Co, which is sensitive to where the other elements are residing [20,21].

The objective of this research effort was to investigate the site occupancies within nickel base superalloys using atom probe tomography and x-ray diffraction. The strategy was to use chemical composition data and lattice positions provided by atom probe tomography to augment x-ray diffraction data. Contrary to previous research efforts employing x-ray diffraction, synchrotron beam energies were controlled to provide different contributions from elements corresponding to the different excitation values. The experimental intensities were compared with modeled results to attempt at providing optimized site occupancies.

Experimental Procedures

For this research, the commercial material Rene88was used because it is a successful commercially relevant alloy with a low g/g' misfit. The alloy has the following composition (at%): 18.02Cr – 13.00Co – 4.74Ti – 4.45Al – 2.48Mo – 1.21W – 0.46Nb , remaining Ni. Samples were cut from a disk produced and tested under work supported by the Defense Advanced Research Projects Agency [32], and solutionized at 1150C for 30 minutes, followed by cooling at at 24 degrees C/minute and then aged at 760 degrees C for 200 hours, and air cooled.

The segregation of elements between the g and g' phases, and the chemical composition within the phases was provided by atom probe tomography (APT). Sharp pointed samples with a

tip radius in the range of 50-100 nm were prepared using standard electropolishing techniques as well as via ion-beam polishing carried out in a dual-beam focused ion beam (FIB) instrument. Experiments were conducted using a LEAP 3000 local electrode atom probe (LEAP^{TM}) system from Cameca, Inc. The system was operated in the electric-field evaporation mode at a temperature of 60K. The evaporation rate varied between 0.5%-1.0% with a pulsing voltage of 20% of the steady state voltage. The IVAS 3.0 system from Cameca, Inc. was used for data analysis.

Anomalous x-ray scattering measurements were performed on beamline 33-BM-C [33,34] at the Advanced Photon Source of the Argonne National Laboratory. This beamline effectively focuses up to 4 mrad of the horizontal fan to a relatively small focal spot (the cross-section area is 1.0×0.5 mm^2) with high (~10^{12} ph/s/100mA) flux at the sample surface [35]. Tuning the incident photon energies to the K-edge of an element causes a significant decrease in the true (f') and imaginary (f") parts of the scattering factor $f = f' + if''$ of the element without significantly altering the scattering factors of the other elements(figure 1). Here i is the imaging unit ($i^2 = -1$). This allows estimation of the contribution of a such suppressed element in the intensities of Bragg's peaks. The incident energy was tuned to E_1 = 5989 eV, E_2 = 7709 eV, E_3 = 8333 eV and E_4 = 18986 eV, which corresponded to the resonance absorption for Cr, Co, Ni and Nb atoms, respectively (Figure 1) [36]. The f' and f" values for the alloying elements at these resonance energies and the scattering angle $\Theta = 0$ are given in Table 1. The Q dependences of f' for different elements at room temperature are given in [37]. To tune the energy, an elemental foil was placed in the incident beam path and the intensity as a function of energy was measured from a forward detector and normalized to the ion chamber prior to the foil. The samples were fixed at a grazing angle in χ between 7° and 15° to maximize the size of the beam on the sample and the intensity of the scattered beam. The effective X-ray excited surface area was estimated to be ~2-4 mm^2, depending on the glazing angle. A reference scan at the energy of E_5 = 8049 eV, which corresponds to the Cu $K_{\alpha 1}$ radiation (λ = 1.54056 Å) and at which the scattering factors of Co, Cr and Ni are almost the same (see figure 1 and Table 1), were obtained using a Rigaku 2500 diffractometer, with the beam cross-section area of 12.5 mm^2.

Table 1. X-ray scattering factors of given elements at different wavelength energies and Q = 0°.

Beam Energy, eV	5989	7709	8049	8333	18986

Wave length, Å	2.0701	1.6083	1.54056	1.4879	0.6530
	Scattering factors, *f'* / *f"*				
Al	13.30 /0.426	13.21 / 0.263	13.20 / 0.240	13.20 / 0.226	13.05 / 0.043
Co	25.69 / 0.745	**15.88 / 3.794**	24.68 / 3.549	25.32 / 3.382	27.35 / 0.827
Cr	**12.92 / 0.467**	23.68 / 2.616	23.85 / 2.429	23.95 / 2.304	24.30 / 0.525
Mo	42.19 / 4.566	42.03 / 2.957	41.97 / 2.733	41.93 / 2.585	39.52 / 0.605
Nb	41.18 / 4.181	40.96 / 2.701	40.90 / 2.494	40.86 / 2.357	**29.37 / 3.745**
Ni	26.89 / 0.895	25.73 / 0.568	24.91 / 0.522	**16.70 / 0.49**	28.36 / 0.964
Ti	21.30 / 3.045	22.18 / 2.011	22.24 / 1.860	22.28 / 1.759	22.26 / 0.385
W	70.38 / 9.155	69.29 / 6.175	68.95 / 5.746	68.67 / 5.459	73.57 / 5.890

Bragg's Peak Intensity Simulation

The integrated intensity (peak area) of a diffraction peak for the *hkl* family of planes in a single phase (γ or γ') is give by the following equation [38]:

$$I_{hkl} = A \times LP(\Theta) \times M_{hkl} \times \left|F_{hkl}(\Theta)\right|^2 \qquad (1)$$

where A is a constant containing experimental and materials parameters, $LP(\Theta)$ is the Lorentz-Polarization factor, M_{hkl} is the multiplicity factor, and $F_{hkl}(\Theta)$ is the total complex structure factor, which is given by:

$$F_{hkl}(\Theta) = \sum_{j=1}^{N} f_j(\Theta) \exp\left[2\pi i\left(hx_j + ky_j + lz_j\right)\right] \qquad (2)$$

In (2), x_j, y_j, and z_j are the coordinates of an element j in real space of the crystal lattice, and N is the number of elements in the crystal. For a conventional X-ray powder diffraction, $LP(\Theta) = \frac{1+\cos^2(2\Theta)}{8\sin^2\Theta\cos\Theta}$. In the case of synchrotron X-ray, radiation is essentially fully polarized in the axial direction and $LP(\Theta) = \frac{1}{4\sin^2\Theta\cos\Theta}$.[39]

For the face-centered-cubic structure the atomic coordinates are [0,0,0], [0.5,0.5,0], [0.5,0,0.5], and [0,0.5,0.5]. For the random solid solution (RSS), Equation (2) yields:

$$F_{hkl}^{RSS}(\Theta) = \langle f(\Theta)\rangle\left[1 + (-1)^{h+k} + (-1)^{k+l} + (-1)^{h+l}\right] \qquad (3)$$

Here $\langle f(\Theta)\rangle$ is the concentration weighted average of the scattering factors of the elements presented in the RSS. Equation (3) is non-zero when h, k, and l are either all even or all odd.

Bragg reflections are only observed for the (111), (200), (220), (311), and so forth planes and their integrated intensities are given by the following Equation (4):

$$I_{hkl}^{RSS} = 16 A_{hkl} M_{hkl} \left(\langle f'_{hkl} \rangle^2 + \langle f''_{hkl} \rangle^2 \right) \quad (4)$$

Here $A_{hkl} = A \times LP(\Theta_{hkl})$, and Θ_{hkl} is the scattering angle at the (h,k,l) diffraction peak. Other reflections are not observed due to the destructive interference of the atoms in the crystal cell positions.

For the ordered FCC solid solution [e.g. γ' ($AlNi_3$) phase], in which some alloying elements are located at the corners (A sites) and other elements are located at the centers of the faces (B sites) of the crystal lattice, the intensities of both fundamental peaks, $I_{Fhkl}^{\gamma'}$, (h, k, and l are either all even or all odd) and super-lattice peaks, $I_{Shkl}^{\gamma'}$, (at least one of h, k, and l is even and at least one is odd) are in general non-zero and given by:

$$I_{Fhkl}^{\gamma'} = A_{hkl} M_{hkl} \left[\left(\langle f'_A \rangle + 3 \langle f'_B \rangle \right)^2 + \left(\langle f''_A \rangle + 3 \langle f''_B \rangle \right)^2 \right] \quad (5)$$

$$I_{Shkl}^{\gamma'} = A_{hkl} M_{hkl} \left[\left(\langle f'_A \rangle - \langle f'_B \rangle \right)^2 + \left(\langle f''_A \rangle - \langle f''_B \rangle \right)^2 \right] \quad (6)$$

Here $\langle f'_j \rangle = \dfrac{\sum_{i=1}^{N} n_i^j c_i f'_i}{\sum_{i=1}^{N} n_i^j c_i}$ and $\langle f''_j \rangle = \dfrac{\sum_{i=1}^{N} n_i^j c_i f''_i}{\sum_{i=1}^{N} n_i^j c_i}$ are the concentration-averaged structure factors of elements located in the *j* site (*j* = A or B), c_i is the concentration of element *i* in the γ' phase, and n_i^j is the fraction of element *i* in the site *j* ($n_i^A + n_i^B = 1$). By fitting the simulated peak intensities to the experimental ones, one can estimate the fractions of the given elements in A and B sites in the γ' phase.

Results and Discussion

The resulting microstructures, from the slow-cooled and slow-cooled plus aged Rene 88 samples are shown in Figure 2. The slow cooled heat treatment formed a bi-modal distribution of γ' precipitates on cooling (2a) which upon aging formed both acicular γ' structures (about 200 nm average diameter) and smaller coherent circular γ' (12 nm average diameter) (2b). The

images were obtained using EFTEM techniques employing the Cr M edge in the energy-loss spectroscopy spectrum.

The results indicate the clear segregation of heavier elements to the γ matrix, and the segregation of Ti, Al, and Nb, to the γ' precipitate. The interface width appears to widen as the material is cooled at a slower rate, and aged for longer time, as reported elsewhere [28]. The results for the sample aged for 200 hours did not contain data from secondary precipitates, only teritiary γ' and γ. Fortunately, a sample cooled under the same conditions yet aged for only 50 hours provided both tertiary and secondary γ' data. In addition, previous research indicated only slight γ' composition changes within the slow cooled samples when aged past 50 hours. The composition of the sample compared favorably to equilibrium compositions predicted using Pandat™ software.

Table 2. Composition (in at.%) of γ' and γ phases for the SC200 samples. Data was obtained using atom probe tomography [40,41].

(atomic%)	Al	Co	Cr	Nb	Ni	Mo	Ti	W	C
γ'	9.8	8.08	2.44	3.54	61.06	2.74	11.33	0.44	0.24
γ	4.58	15.32	21.14	2.27	43.13	6.23	2.31	2.38	1.43

Figure 3 illustrates X-ray diffraction patterns of the SC200 alloy sample taken at two different X-ray energies, E_2 = 7709 eV (Figure 3a) and E_5 = 18986 eV (Figure 3b). The patterns are plotted in coordinates 2Θ versus logarithm intensity (number of counts). It can be clearly seen that the intensities of super-lattice peaks (identified by a letter 's' in the figures) are energy dependent, which is evidently due to an anomalous X-ray absorption by a certain alloying element (i.e. Cr, Co, Ni or Nb) at a given radiation energy. In particular, at the energy E_5 = 18986 eV, at which the structure factor of Nb is noticeably suppressed, the super-lattice peaks are much stronger than at E_2 = 7709 eV, corresponding to the Co structure factor suppression (see Table 1). The fundamental peaks are also energy dependent. For example, at E_2 = 7709 eV the intensity of the (220) peak is higher than the intensity of the (111) peak, while at E_5 = 18986 eV an opposite trend is seen. It should be noted that, because of very close lattice parameters of the γ and γ' phases, each fundamental peak presented in the diffraction patterns is the sum of the respective fundamental diffraction peaks from these two phases. At the same time, the super-lattice peaks

belong to the ordered γ' phase. The presence of at least 8 super-lattice peaks in the diffraction pattern at E_5 = 18986 eV allowed the lattice parameter of the γ' phase to be determined as $a_{\gamma'}$ = 3.596 ± 0.001 Å.

The integrated intensities of the diffraction peaks were determined after removing the background and using a Peak Fit program. The peak intensities were then normalized by assigning the intensity value of 100% to the (111) peak. Such normalization procedure allowed exclusion of any beam alignment effects on the peak intensities at different radiation energies, so that only materials parameters affected the intensities of the same peaks at different energies. The intensities of the first seven diffraction peaks are given in Table 3. It can be seen that the intensity of the (200) fundamental peak is maximum (91.4%) at E_1 = 5989 eV and minimum (17.6%) at E_2 = 7709 eV. At the same time, the intensity of the (220) fundamental peak is maximum (172.4%) at E_2 = 7709 eV and it decreases to 11.3% with an increase in the radiation energy to E_5 = 18986 eV. Such dramatic variations in the intensities of the fundamental peaks on the radiation energy for the same sample are unlikely due to suppression of the scattering factors of the given alloying elements. Most likely these intensity variations were due to a small beam size relative to the γ grain size and an artificial 'texture' effect due to insufficient amount of grains inside the beam. Thus small changes in the beam location on the sample surface could lead to different diffraction conditions. This 'texture' effect can however be reduced allowing the analysis of the effect of suppression of the structure factors of the given elements on the peak intensities, if relative intensities of the same family of the diffraction peaks are analyzed, e.g I_{100}/I_{200} and I_{110}/I_{220}. These relative intensities are given in last two rows of Table 3.

Table 3. Integrated intensities [normalized to the (111) peak intensity, which is taken as 100%] of several diffraction peaks as a function of the X-ray beam energy. The relative intensities of the same family peaks are also given in two last rows.

Beam Energy, eV	5989	7709	8049	8333	18986
Suppressed Element	Cr	Co		Ni	Nb
(100)s	0.29	0.29	0.27	0.03	1.28
(110)s	0.34	0.50	0.22	0.03	0.86
(111)	100	100	100	100	100

(200)	91.40	17.6	35.70	74.90	52.10
(210)s	-	0.15	0.07	0.00	1.09
(211)s	-	0.00	0.00	0.00	0.36
(220)	-	172.4	18.00	14.80	11.30
$I_{(100)s}/I_{(200)}\times100\%$	0.32	1.65	0.76	0.04	2.46
$I_{(110)s}/I_{(220)}\times100\%$	-	0.29	1.22	0.20	7.61

Using the peak intensity data given in Table 3 and knowing the effect of the radiation energy on the structure factors of the alloying elements (Table 1) one can speculate on which site (aluminum, A, or nickel, B) of the γ' lattice the alloying elements likely occupy. Among all the alloying elements, Al has the lowest structural factor ($f' \approx 13.2$), which remains nearly constant within the studied radiation energy range (Figure 1). The normal scattering factors of other alloying elements are considerably higher than that of Al. Therefore, in accord to Equation (6), suppression of the structure factor of a particular element, without changing the structure factors of other elements, should lead to a decrease in the intensity of the super-lattice peaks if this element preferably occupies B sites. On the other hand, if an alloying element preferably shares the site positions with Al, the intensities of the super-lattice peaks should increase. The suppression of the structure factor of an alloying element should also lead to a decrease in the intensity of fundamental peaks, in accord to Equations (4) and (5). Equation (5) however predicts that the decrease in the fundamental peak intensities should be more noticeable after suppression of elements located in the B sites.

At $E_3 = 8049$ eV, the anomalous scattering of the alloying elements is absent or very weak. Moreover, f' values of Cr, Co and Ni are nearly the same (~23.9-24.9) and f' of Nb and Mo are ~41. Therefore, the relative intensities $I_1 = I_{(100)s}/I_{(200)} \times100\% = 0.76\%$ and $I_2 = I_{(110)s}/I_{(220)} \times100\% = 1.22\%$ observed at $E_3 = 8049$ eV can be taken as the reference values of the condition without anomalous scattering. At $E_4 = 8333$ eV, the structure factor of Ni is considerably suppressed and becomes very close to that of Al, while the structure factors of other elements remain almost unchanged. This results in a considerable decrease in I_1 and I_2 to the values of 0.04% and 0.20%, respectively. This considerable decrease in the relative intensities of the super-lattice peaks due to the suppression of Ni structure factor is in full agreement with the fact

that Ni and Al occupy different sites of the γ' lattice and also in agreement with Equations (4) - (6).

At E_1 = 5989 eV, the structure factor of Cr is suppressed to below that of Al and this is accompanied with a decrease in I_1 to 0.32%. This intensity is more than twice lower than the intensity I_1 = 0.76% at E_3 = 8049 eV, when the anomalous scattering is absent. This result likely indicates that Cr is located in Ni (B) sites of the γ' lattice. The structure factor of Co is suppressed at E_3 = 7709 eV and this causes a considerable increase in I_1 (to 1.65%), but a more pronounced decrease in I_2 (to 0.29% relative to I_2 = 1.22% observed in the neutral condition at E_3 = 8049 eV). Because of such a different response of the (100) and (110) super-lattice peaks on the suppression of Co, we cannot say for sure if Co is located in Ni or Al sites. It is likely that this element shares both these sites. Finally, suppression of the scattering factor of Nb at E_5=18986 eV causes a considerable increase in the intensities of the super-lattice peaks, which is an unambiguous indication that this element shares sites with Al.

Unfortunately, the anomalous scattering conditions for other alloying elements (i.e. Ti, Mo and W) were not studied and thus the site occupancies of these elements were not identified directly from the experimental data in this work. Additional scattering experiments at the energies corresponding to the Ti, Mo and W absorption edges are required to identify what γ' phase sites these elements prefer to occupy. At the same time, it is well established that Ti prefers to occupy the same lattice positions as Al [ref.]. If we assume that all Al (9.80 at.%), Nb (3.54%) and Ti (11.3) in the γ' phase occupy A sites, then the concentration of these elements in the A sites would be 24.67%, i.e. all A sites would be taken by these elements and there would be no possibility for other elements to take these positions. Therefore, all other elements, including Cr and Co, should share the positions with Ni in B sites. Our synchrotron results however indicate that Co (8.08%) may occupy both A and B sites. In the case of no preferential site occupancy, about 2% of Co would be located in the A sites and thus approximately the same amount of Al, Ti and/or Nb should move to the B sites.

To provide a comparison between APT and XRD techniques, data from a slow cooled sample, aged for 50 hours at 760 degrees C [40], was oriented with the (002) planes relatively perpendicular to the electrode and detector was used to investigate site preferences. The sample provided excellent resolution of (002) planes not detectable in the 200 hour aged sample.

Plotting the composition of different elements versus distance within a large γ' precipitate provided a method for comparing which elements were occupying the nickel and aluminum sublattice positions. As shown in Figure 4, the Ni and Al elements clearly occupy alternate lattice positions relative to the sampling direction. The elements Ti and Cr also appear to occupy the same positions as Al, although there is a slight shift in the intensity position created by differences in evaporation rates. The element Co did not show a strong match with either the Ni or Al sites, indicating there was no strong preference for site occupancy in either sublattice.

The results for the site occupancy x-ray diffraction model do not match the experimental results from the APT slow cooled 50 hour sample, or results provided in literature [19,21] which indicate that Cr prefers to occupy the Al sublattice positions. One possible explanation is that other alloying elements may share a stronger preference for this position given neighbor-neighbor interactions. The analysis based on the x-ray data did show that Nb and Ti prefer the Al position (at least partially), and that Mo and W prefer the Ni sublattice site, in agreement with published data [21]. Another possibility for the model discrepancy may reside with the volume fraction and/or chemistry data used in the fitting model. Because the values relied on APT results, which by nature involve a limited amount of material, the calculated volume fraction and chemistries may not be representative of the bulk material. To test for sensitivity, the volume fraction value used in the calculations was altered with only minimum impact on the results.

Conclusions

1. The use of monochromated beam energies allowed the modeling of site selection in water quenched and slow cooled Rene88DT samples. The use of APT techniques provided composition data critical for modeling the potential lattice locations within γ'.

2. Analysis of the synchrotron data identified the preference for niobium to reside at the Al sublattice sites, and titanium to reside at least partially on the nickel sites within the ordered g'. Preliminary results indicate that Mo, W, Cr, and Co reside on nickel sites within the ordered g', although only limited beam energies were used to generate the intensities.

3. Careful alignment of the APT samples provided identification of the (100) planes and allowed comparison of Ti, Ni, Al, and Cr site preferences by overlaying composition versus position data. Both Ti and Cr preferentially resided at Al sublattice sites within the ordered γ'. Cobalt did not appear to show a strong specific site preference. However, the small amount of Co present in the γ' phase coupled with detection efficiency in the atom probe severely restrict the analysis of this alloying element within the γ' phase.

4. Additional data, employing synchrotron energies that will suppress remaining elements, are required to complete the comparisons of the diffraction intensities. APT characterization with samples oriented to align specific planes within γ' relative to the detector are also required to provide experimental validation and secondary γ' composition.

References

1 Reed RC, The superalloys, fundamentals and applications. Cambridge: Cambridge University Press (2006) p. 236.
2 Telesman J, Kantzos P, Gayda J, Bonacuse PJ, Presecenzi A, In: Superalloys 2004. Warrendale, PA: TMS Publications (2004) p. 215.
3 Stoloff NS. In: Superalloys II. New York: John Wiley (1987) p. 61.
4 Schafrik RE, Walston , In: Superalloys 2008, TMS Publications (2008) p. 3.
5 Guedou JY, Lecallier A, Naze L, Caron P, Locq D, In Superalloys 2008, TMS Publications (2008) p. 21.
6 Babu SS, Niller MK, Vitek JM, David SA, Acta Mater, 49 (2001) 4149-4160.
7 Singh ARP, Nag S, Hwang JY, Viswanathan GB, Tiley J, Srinivasan R, Fraser HL, Banerjee R, Mat Charact 62 (2001) P. 878.
8 Viswanathan GB, Sarosi PW, Henry MF, Whitis DD, Milligan WW, Mills MJ, Acta Mater, 53 (2005) p. 81.3040.
9 Sondhi SK, Dyson BF, McLean, Acta Mater 52 (2004) p. 1761.
10 Kassner M, Perez-Prado MT, Fundamentals of Creep in Metals and Alloys, Sec Ed, Elsevier Inc (2009)
11 Krueger DD, Kissinger RD, Menzies RD, Wukusick CS, U.S. Patent 4957567, (1990).
12 Parthasararthy TA, Rao SI, Dimiduk DM, In: Superalloys 2004, TMS Publications (2004) p. 887.
13 Wlodek ST, Kelly M, Alden DA, In: Superalloys 1996, TMS Publications (1996) p.129-136.
14 Tiley J, Viswanathan GB, Srinivasan R, Banerjee R, Dimiduk DM, Fraser HL, Acta Mater 57 (2009) p. 2538-2549.
15 Ardell AJ, Ozolins V, Nat Mater, 4 (2005) p. 309.
16 Muralidharan G, Richardson Jr JW, Epperson JE, Chen H, Scripta Mat v 36, n 5 (1997) p. 543.

17 Tiley J, Srinivasan R, Banerjee R, Viswanathan GB, Toby B, Fraser HL, Mat Sci and Tech, v 25, n 11 (2009) p. 1369.
18 Chaudhari M, Singh A, Gopal P, Nag S, Viswanathan GB, Tiley J, Banerjee R, Du J, Phil Mag Let, in press (2012).
19 Guard RW, Westbrook JH, Transactions of the Metallurgical Society of AIME, v 215, (1959) p. 807.
20 Jiang C, Gleeson B, Scripta Mat 55 (2006) p. 433.
21 Wanderka N, Glatzel U, Mater Sci Eng A203 (1995) p. 69.
22 Blavette D, Bostel A, Acta Mater v 32, n 5 (1984) p. 811.
23 Blavetti D, Cadel E, Deconihout B, Material Characterization, 4 (2000) p. 133-157.
24 Miller MK, Cerezo A, Hetherington MG, Smith GDW, Atom probe field in microscopy, Oxford University Press (1996) p. 476-83.
25 Miller MK, Micron, 32 (2001) p. 757-764.
26 Seidman DN, Sudbrack CK, Yoon KE, JOM, 58 (2006) p. 34-9.
27 Yoon KE, Noebe RD, Seidman DN, Acta Mater, v 55, iss 4 (2007) p. 1159.
28 Hwang JY, Banerjee R, Tiley J, Srinivasan R, Viswanathan GB, Fraser HL, Met Mat Trans A, v 40A (2009) p. 24.
29 Olson GB, jou HJ, jung J, Sebastian JT, Misra A Locci I, Hull D, In: Superalloys 2008, TMS Publications (2008) p. 923.
30 Porter III WJ, Li K, Caton MJ, Jha S, Bartha BB, Larsen JM, In: Superalloys 2008, TMS Publications (2008) p. 541.
31 Tiley J, Viswanathan GB, Hwang JY, Shiveley A, Banerjee R, Mat Sci and Eng A 528 (2010) p. 32.
32 Littles Jr JW, Petit RG, Schirra JJ, Cowles BA, Holmes RQ, Russ SM, et al., In: Materials damage prognosis. Warrendale, PA: TMS Publications (2005) p. 23.
33 Karapetrova E, Ice G, Tischler J, Hong H, Zschack P, Nuclear Instruments and Methods in Physics Research A, 649 (2011) 52-54.
34 http://www.aps.anl.gov/Beamlines/Directory/showbeamline.php?beamline_id=83.
35 Sparks Jr. CJ, Ice GE, Wong J, Batterman BW, Nucl. Instr. Meth. 195 (1982) 73.
36 Henke BL, Gullikson EM, Davis JC, Atomic Data and Nuclear Tables, 54 (1993) p. 181.
37 Waasmaier D, Kirfel A, Acta Crystall A51 (1995) p. 416
38 Graef MD, McHenry ME, Structure of Materials: An Introduction to Crystallography, Diffraction, and Symmetry (Cambridge University Press, Cambridge, 2007) p. 305.
39 Stone HJ, Peet MJ, Bhadeshia HKDH, Proc. R. Soc. A 464 (2008) 1009-1027.
40 Hwang JY, Nag S, Singh ARP, Srinivasan R, Tiley J, Viswanathan GB, Fraser HL, Banerjee R, Metall. Mater. Trans. 40A (2009) 3059-3068.
41 Srinivasan R, Banerjee R, Hwang JY, Viswanathan GB, Tiley J, Dimiduk DM, Fraser HL, PRL 102 (2009) 086101.

Figures:

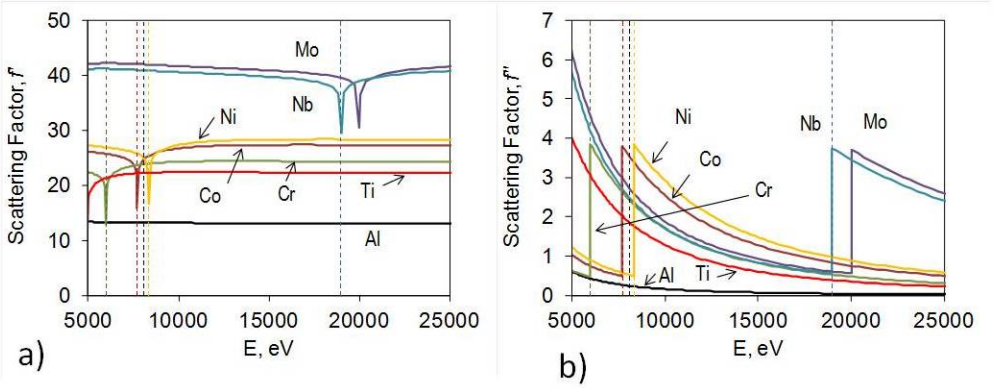

Figure 1. X-ray scattering factors (a) f' and (b) f'' for Al, Co, Cr, Mo, Nb, Ni and Ti in the X-ray energy range of 5000 to 25000 eV and Q =0° [36]. The vertical lines correspond to the energies used in this work.

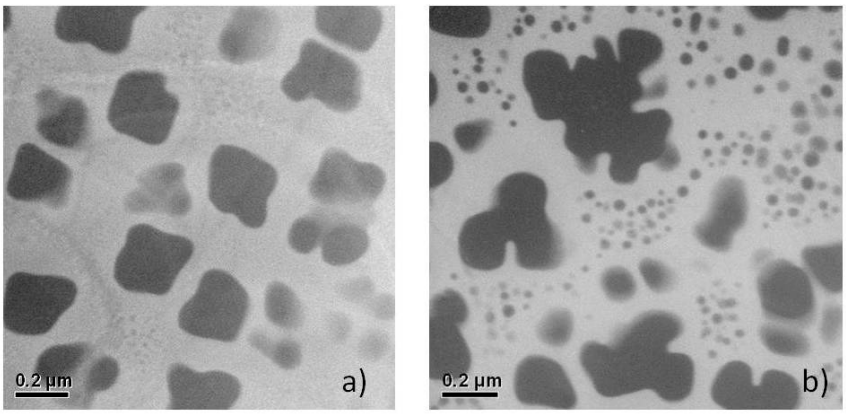

Figure 2: Energy filtered transmission electron microscopy images, a) sample as cooled, b) sample aged for 200 hours at 760 degrees C. The ordered γ' precipitates appear dark in the image compared to the lighter γ matrix.

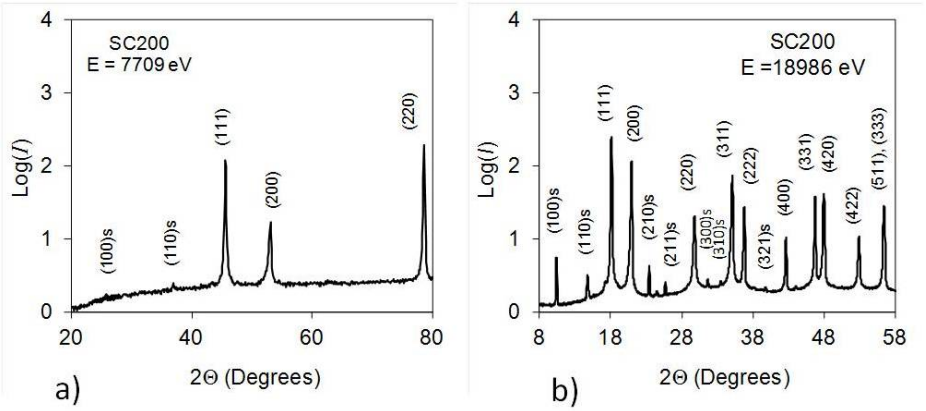

Figure 3. X-ray diffraction patterns of a slow cooled Rene88 sample (SC200). The beam energy is (a) E= 7709 eV and (b) E = 18986 eV.

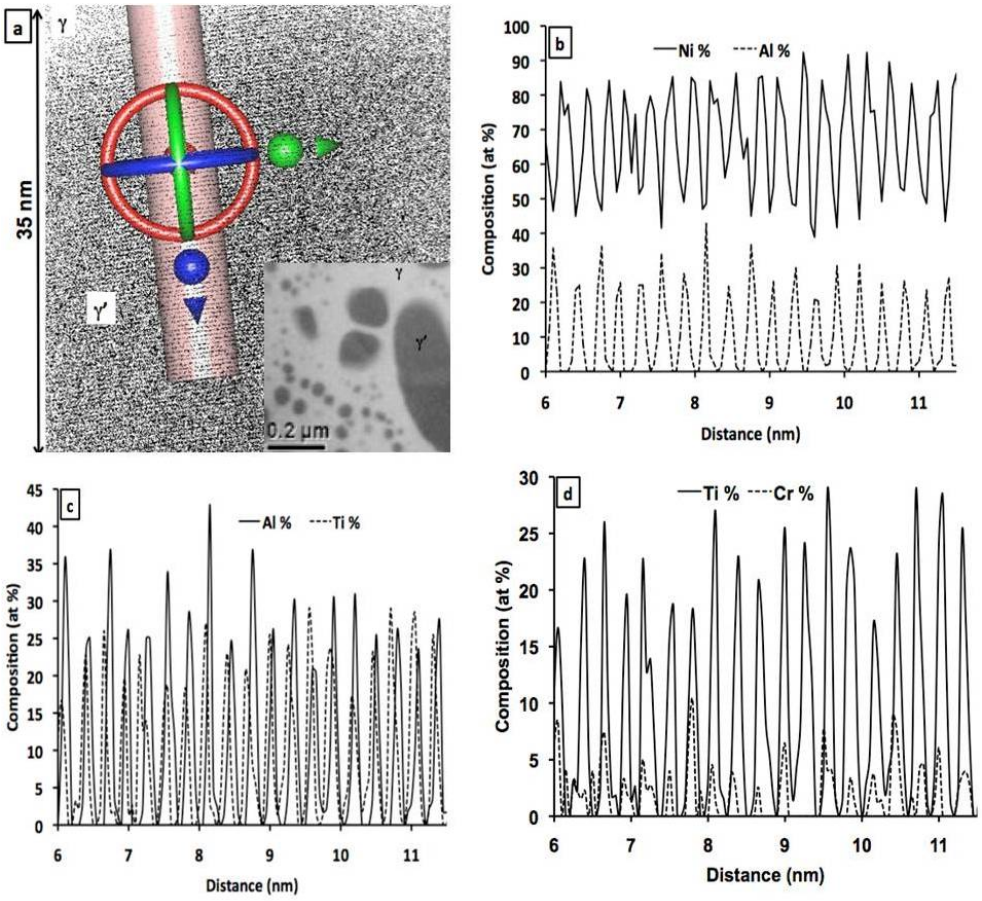

Figure 4: a) sampling area within g matrix, inset shows γ and γ' phases, b) composition plot for Ni and Al and Al, c) composition plot for Al and Ti, d) composition plot for Ti and Cr.